On the Bandwidth Capabilities of Connected Slot Arrays

Christos Monochristou, Mattia Maggi, Ronan Sauleau, Mauro Ettorre

On the Bandwidth Capabilities of Connected Slot Arrays

Christos Monochristou, *Student Member, IEEE,* Shang Xiang, *Member, IEEE,* Mark Holm, *Senior Member, IEEE,* Ronan Sauleau, *Fellow, IEEE,* and Mauro Ettorre, *Fellow, IEEE*

***Abstract*—This work explores the bandwidth limits of connected slot arrays, focusing on their low-frequency bound. We show how the ground plane, present in this structure to ensure unidirectional radiation, places a limit on their operation in terms of active reflection coefficient at lower frequencies. In particular, a low-frequency approximation of the active reflection coefficient of a representative connected slot array is derived based on a Green's function formulation and an equivalent circuit model of the array. The design parameters of the array unit-cell are taken into account and their influence on the proposed limit is analyzed. Finally, the low-frequency approximation reveals the impact of surface waves when scanning over the E-plane of the array. A solution to overcome such an issue is proposed. It considers the introduction of vertical metallic walls within the substrate supporting the slots of the array. The proposed low-frequency bound is modified accordingly to further highlight the benefits of this solution.**

***Index Terms*—Connected arrays, slot arrays, bandwidth, bounds, surface waves.**

I. Introduction

PHASED arrays are a very appealing solution for a wide range of applications where the agility of the radiating unit, its form factor, and its operating band are key parameters.

In the last decades, different array architectures have been proposed, providing ultra-wideband (UWB) operation and wide fields of view (FoV). The majority of these arrays are an implementation of Wheeler's current sheet concept [1], which adopt non-resonant elements with high mutual coupling to substantially enlarge their bandwidth. Two members of this group are the connected dipole arrays [2] and the Tightly Coupled Dipole Arrays (TCDA) [3], both presenting large bandwidths up to 3:1 and 10:1 respectively, low cross-polarization levels, and low profiles ($h \in [0.1\ 0.2]\cdot\lambda_0^{\text{lo}}$, h being the total profile thickness and λ_0^{lo} the free space wavelength at the minimum frequency of operation). The Continuous Transverse Stub (CTS) array is also part of the same class and has been proven to deliver comparable performance with over $40\,\%$ bandwidth [4], albeit with total thickness over λ_0^{lo} [5]. On the other hand, the Planar Ultrawideband Modular Antenna (PUMA) array [6] and the connected slot array [7] have demonstrated bandwidths between 3:1 and 6:1 with a low-profile structure ($h \in [0.07\ 0.13] \cdot \lambda_0^{\text{lo}}$).

Manuscript received June 17, 2023; revised September 18, 2023. This work was supported in part by Huawei Technologies (Sweden) AB.

C. Monochristou, M. Ettorre and R. Sauleau are with Univ Rennes, CNRS, IETR (Institut d'Electronique et des Technologies du numéRique) - UMR 6164, F-35000, Rennes, France (e-mail: christos.monochristou@univ-rennes.fr, mauro.ettorre@univ-rennes.fr, ronan.sauleau@univ-rennes.fr).

S. Xiang and M. Holm are with Radio Basestation Systems Department, Huawei Technologies (Sweden) AB, Gothenburg, Sweden (e-mail: shang.xiang1@huawei.com, mark.holm@huawei.com).

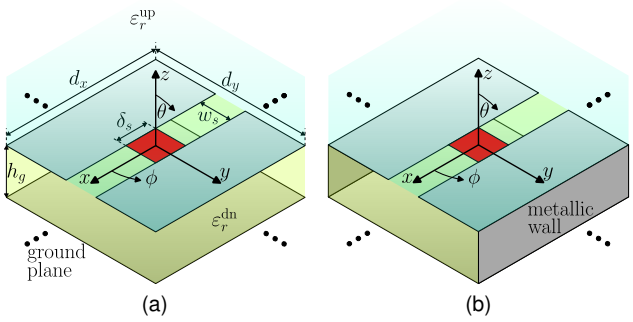

Fig. 1. (a) Unit-cell of a connected slot array backed by a ground plane. (b) Modified connected array unit-cell with metallic walls in the substrate parallel to the slot direction. The delta-gap excitation is depicted as red.

In order to gain insight into the physical bounds and quantify the trade-off between the bandwidth and the thickness of different types of antenna arrays, various approaches have been already explored. In [8], an approximate limit for self-complementary arrays is developed. A minimum Q-factor has been extracted for infinite arrays of cylindrical electric [9] and magnetic [10] sources. [11] analyzes the effect of the array geometry, materials, and FoV on its attainable frequency band for both narrowband and wideband designs. Nevertheless, it accounts only for linearly-polarized arrays in free space, namely without the backing reflector. Finally, generic bandwidth limits for arrays with ground planes have been determined [12] and then extended for structures with arbitrary polarization [13]. Since no previous work is dedicated to connected arrays despite their importance, here we provide a systematic analysis and a low-frequency limit for this array category.

The connected slot array presents a particular interest due to its simple structure and its feed, which is straightforward to design and implement. Consequently, there is a strong incentive to extend the theoretical background regarding their operation as well as to develop connected arrays with broadened bandwidths. The present analysis contributes to both these objectives by rigorously deriving a bandwidth limit, along with a set of guidelines for designing structures able to radiate efficiently at extremely low frequencies. For that purpose, we employ a simplified and realistic geometry of the array along with a framework of consistent assumptions concerning the array environment and the properties of the electromagnetic field at low frequencies. The bandwidth bounds for the active reflection coefficient of the unit-cell are then obtained. The proposed analysis is valid for any connected array architecture

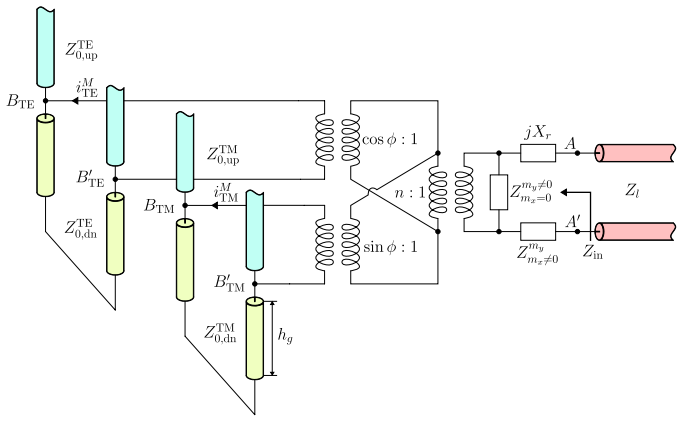

Fig. 2. Equivalent circuit of the unit-cell in Fig. 1 for the fundamental Floquet mode operation ($m_x = m_y = 0$), valid for $d < \lambda_0^{\mathrm{hi}}/2$.

and for steering at arbitrary angles.

II. Connected Slot Unit-Cell

The unit-cell of a connected slot array is illustrated in Fig. 1a, backed by a ground plane for unidirectional radiation. The unit-cell is covered by a homogeneous material characterized by $\varepsilon_r^{\mathrm{up}}$ and the slot is etched on a metallic layer, referred to as the "radiation plane". The substrate, separating the ground plane from the radiation plane, consists of a homogeneous dielectric with relative permittivity $\varepsilon_r^{\mathrm{dn}}$. To simplify the analysis, an ideal delta-gap excitation is considered (in red in Fig. 1). The dielectric radome covering the array is used as a matching layer to enlarge the bandwidth. An alternative is the artificial dielectric layer (ADL) [14], which is less bulky while enabling wider FoV compared to homogeneous radomes. The choice of the radome does not affect the conclusions of this work.

It has already been proven in [15] that a connected slot array in free space with bidirectional radiation can theoretically operate from DC up to the frequency where its periodicity (d) is half a wavelength in free space $(d = \lambda_0^{\mathrm{hi}}/2)$. This is a typical constraint for phased arrays to avoid grating lobes (GLs) while scanning [16] and thus it will be used also here as the upper-frequency limit of the bandwidth

$$f_{\mathrm{hi}} = \frac{c}{2d}, \tag{1}$$

where c is the speed of light in vacuum and d is the largest periodicity of the array in the xy-plane $[d = \max(d_x, d_y)]$.

Due to the introduction of the ground plane below the radiation plane, the antenna response becomes frequency dependent with a lower bound for the operating frequency f_{lo}. Nevertheless, the effect of the backing reflector can be reduced by increasing the dielectric constant or equivalently the electrical density of the medium above the radiation plane [14] with either a homogeneous radome or an ADL. The bandwidth bound produced herein considers the electrically denser medium above the antenna by assuming that the upper hemisphere has an arbitrary relative permittivity $\varepsilon_r^{\mathrm{up}}$ as seen in Fig. 1. This renders a multi-layer impedance transformer unnecessary and allows the derivation of a low-frequency limit analytically.

We consider the Green's function formulation and the equivalent circuit provided in [17] for the connected dipole structure. By duality, the equivalent circuit for the connected slot array, displayed in Fig. 2, can be derived. Z_l is the characteristic impedance of the feeding network at the slot level or, equivalently in our simplified model, it is the internal impedance of the delta-gap excitation. The load jX_r is purely imaginary and represents the reactance introduced by a realistic feed of the slot. This can be also tuned in order to improve the unit-cell operation [18]. The characteristic impedances of the transmission lines modeling the stratification are given by

$$Z_0^{\mathrm{TE}} = \eta \frac{k}{k_z} \tag{2}$$

$$Z_0^{\mathrm{TM}} = \eta \frac{k_z}{k} \tag{3}$$

with k the propagation constant, η the wave impedance, and $k_z = \sqrt{k^2 - k_x^2 - k_y^2}, k_x, k_y$ the cartesian components of the wavevector in the corresponding medium, respectively.

Z_{in} is the active input impedance of the connected slot array and is given as a double infinite sum over the Floquet modes, yielding [17]

$$Z_{\mathrm{in}} = -\frac{d_y}{d_x} \sum_{m_x=-\infty}^{\infty} \frac{\mathrm{sinc}^2\left(k_{xm}\frac{\delta_s}{2}\right)}{\sum_{m_y=-\infty}^{\infty} G_{xx}^{HM}(k_{xm}, k_{ym}) J_0\left(k_{ym}\frac{w_s}{2}\right)}. \tag{4}$$

J_0 is the zeroth order Bessel function of the first kind and the Floquet wavenumbers are defined as $k_{xm} = k_{x0} - 2\pi m_x/d_x$ and $k_{ym} = k_{y0} - 2\pi m_y/d_y$ with $k_{x0} = k_0 \sin\theta\cos\phi$ and $k_{y0} = k_0 \sin\theta \sin\phi$, where k_0 is the propagation constant in free space and θ, ϕ define the observation direction in free space in the spherical coordinate system shown in Fig. 1. In (4), G_{xx}^{HM} corresponds to the term of the dyadic Green's function relating to the x-component of the magnetic field (H_x) radiated by a magnetic current (M) oriented along the x-axis. In planar stratified media, G_{xx}^{HM} can be expressed as

$$\begin{aligned} G_{xx}^{HM}(k_x, k_y) &= G_{xx,\mathrm{up}}^{HM}(k_x, k_y) + G_{xx,\mathrm{dn}}^{HM}(k_x, k_y) \\ &= -\frac{i^M_{\mathrm{TE,up}} k_x^2 + i^M_{\mathrm{TM,up}} k_y^2}{k_x^2 + k_y^2} - \frac{i^M_{\mathrm{TE,dn}} k_x^2 + i^M_{\mathrm{TM,dn}} k_y^2}{k_x^2 + k_y^2}. \end{aligned} \tag{5}$$

The currents at the slot level (at $B_{\mathrm{Tf}}B'_{\mathrm{Tf}}$ in Fig. 2), assuming unitary voltage sources on transmission lines, emerge as

$$i^M_{\mathrm{Tf,up}} = \frac{1}{Z^{\mathrm{Tf}}_{\mathrm{up}}}; \quad i^M_{\mathrm{Tf,dn}} = \frac{1}{Z^{\mathrm{Tf}}_{\mathrm{dn}}}, \tag{6}$$

where $Z^{\mathrm{Tf}}_{\mathrm{up}}$ ($Z^{\mathrm{Tf}}_{\mathrm{dn}}$) is the input impedance for the corresponding Floquet mode at the $z = 0$ plane looking towards $z > 0$ ($z < 0$) and Tf represents either TE or TM.

Following the derivation in [17] for connected dipole arrays, the expressions of the remaining components of the equivalent circuit of Fig. 2 can be derived from (4) for the connected slot unit-cell as

$$Z^{m_y}_{m_x\neq 0} = -\frac{1}{d_x} \sum_{m_x\neq 0} \frac{\mathrm{sinc}^2\left(k_{xm}\frac{\delta_s}{2}\right)}{D(k_{xm})} \tag{7}$$

$$Y_{m_x=0}^{m_y\neq 0} = -\frac{d_x}{d_y}\sum_{m_y\neq 0}\frac{G_{xx}^{HM}(k_{x0},k_{ym})J_0\left(k_{ym}\frac{w_s}{2}\right)}{\mathrm{sinc}^2\left(k_{x0}\frac{\delta_s}{2}\right)} \tag{8}$$

$$n = \sqrt{\frac{d_x J_0\left(k_{y0}\frac{w_s}{2}\right)}{d_y \mathrm{sinc}^2\left(k_{x0}\frac{\delta_s}{2}\right)}}. \tag{9}$$

In the structure in Fig. 2, $Z_{\mathrm{up}}^{\mathrm{Tf}} = Z_{0,\mathrm{up}}^{\mathrm{Tf}}$ and $Z_{\mathrm{dn}}^{\mathrm{Tf}} = jZ_{0,\mathrm{dn}}^{\mathrm{Tf}}\tan k_z^{\mathrm{dn}}h_g$, therefore, the currents (6) become

$$i_{\mathrm{Tf}}^{M} = \frac{Z_{0,\mathrm{dn}}^{\mathrm{Tf}}\tan k_z^{\mathrm{dn}}h_g - jZ_{0,\mathrm{up}}^{\mathrm{Tf}}}{Z_{0,\mathrm{up}}^{\mathrm{Tf}}Z_{0,\mathrm{d}}^{\mathrm{Tf}}\tan k_z^{\mathrm{dn}}h_g}. \tag{10}$$

Then, combining (2), (3), (5), and (10) we can calculate the Green's function for the specific stratification with the ground plane, the substrate, the radiation plane and the superstrate above it:

$$G_{xx,\mathrm{gp}}^{HM}(k_x,k_y) = -\frac{1}{\eta_0 k_0}\left[\frac{k_{\mathrm{up}}^2-k_x^2}{k_z^{\mathrm{up}}} - j\cot(k_z^{\mathrm{dn}}h_g)\frac{k_{\mathrm{dn}}^2-k_x^2}{k_z^{\mathrm{dn}}}\right]. \tag{11}$$

Substituting (11) in (4), we obtain the active input impedance of our structure (Fig. 1a)

$$Z_{\mathrm{in}}^{\mathrm{gp}} = \frac{\eta_0 k_0 d_y}{d_x}\sum_{m_x=-\infty}^{\infty}\mathrm{sinc}^2\left(k_{xm}\frac{\delta_s}{2}\right) \cdot \frac{1}{\sum_{m_y=-\infty}^{\infty}\left[\frac{k_{\mathrm{up}}^2-k_{xm}^2}{k_{zm}^{\mathrm{up}}} - j\frac{k_{\mathrm{dn}}^2-k_{xm}^2}{k_{zm}^{\mathrm{dn}}}\cot k_{zm}^{\mathrm{dn}}h_g\right]J_0\left(k_{ym}\frac{w_s}{2}\right)}. \tag{12}$$

III. Low-Frequency Approximation

We now introduce a low-frequency approximation of (12). When $f \to 0$, the fundamental Floquet modes ($m_x = m_y = 0$) accurately describe the structure's behavior. Furthermore, in this frequency region, the arguments of the sinc and Bessel functions tend to zero, thus the approximation $\mathrm{sinc}^2(k_{x0}\delta_s/2)/J_0(k_{y0}w_s/2) \cong 1$ can be employed with an error smaller than 1 %. The active input impedance takes the form

$$Z_{\mathrm{in,lf}}^{\mathrm{gp}} = \frac{A}{B - jC\cot k_z^{\mathrm{dn}}h_g} \tag{13}$$

$$A = \frac{\eta_0 d_y}{d_x} \tag{14}$$

$$B = \frac{\varepsilon_r^{\mathrm{up}} - \sin^2\theta\cos^2\phi}{\sqrt{\varepsilon_r^{\mathrm{up}} - \sin^2\theta}} \tag{15}$$

$$C = \frac{\varepsilon_r^{\mathrm{dn}} - \sin^2\theta\cos^2\phi}{\sqrt{\varepsilon_r^{\mathrm{dn}} - \sin^2\theta}}. \tag{16}$$

The circuital representation in Fig. 2 remains the same, except for $Z_{m_x\neq 0}^{m_y}$ and $Z_{m_x=0}^{m_y\neq 0}$ which become a short- and open-circuit respectively, whereas the transformer is simplified to $n = \sqrt{d_x/d_y}$. In Fig. 3(a) the approximate expression (13) is compared to the exact solution (12), while Fig. 3(b) provides the contribution of the higher order Floquet modes

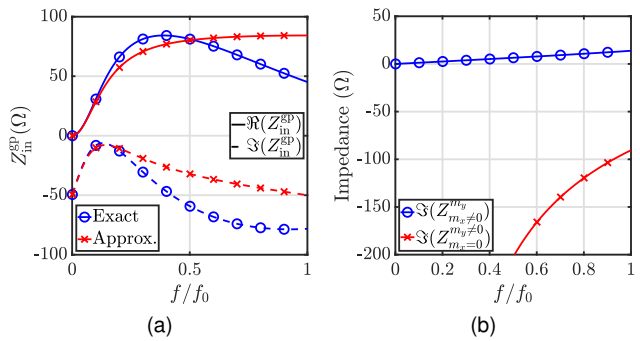

Fig. 3. (a) Active input impedance ($Z_{\mathrm{in}}^{\mathrm{gp}}$) of the unit-cell in Fig. 1a. (b) Contribution of the higher order Floquet modes to $Z_{\mathrm{in}}^{\mathrm{gp}}$. The parameters of the unit-cell are listed in Table I.

to the active input impedance, which is ignored in the low-frequency approximation. Considering that the analysis of the connected slot unit cell [17] assumes that all Floquet modes except the fundamental are in cut-off, $Z_{m_x\neq 0}^{m_y}$ and $Z_{m_x=0}^{m_y\neq 0}$ are pure reactances. The former term is connected in series and is evidently very low with a negligible effect on $Z_{\mathrm{in}}^{\mathrm{gp}}$. The latter ($Z_{m_x=0}^{m_y\neq 0}$), on the other hand, is connected in parallel and, although at low frequencies it assumes large values, for $f > 0.5f_0$ it becomes comparable to $Z_{\mathrm{in}}^{\mathrm{gp}}$, where f_0 is the design frequency of the array and usually equals f_{hi}. Consequently, the increased reactive energy of the Floquet modes with $m_x = 0$ and $m_y \neq 0$ at high frequencies defines the limit of the proposed approach.

In order to derive a frequency limit, a metric of evaluation must be defined. An intuitive approach is to set an upper limit to the absolute value of the active reflection coefficient

$$|\Gamma_{\mathrm{act}}| = \left|\frac{Z_{\mathrm{in}} - Z_l}{Z_{\mathrm{in}} + Z_l}\right| = \left|\frac{z_{\mathrm{in}} - 1}{z_{\mathrm{in}} + 1}\right| \tag{17}$$

with $z_{\mathrm{in}} = Z_{\mathrm{in}}/Z_l$ the normalized input impedance. Following a procedure similar to the Smith chart's mapping [19], it is straightforward to conclude that, for a given $|\Gamma_{\mathrm{act}}|^2 = \gamma$, a circle is drawn on the complex plane defined by $z_{\mathrm{in}} = r_{\mathrm{in}} + jx_{\mathrm{in}}$. The circle's equation is

$$z_{\mathrm{in}}\overline{z_{\mathrm{in}}} - \kappa(z_{\mathrm{in}} + \overline{z_{\mathrm{in}}}) + 1 = 0 \tag{18}$$

$$\kappa = \frac{1+\gamma}{1-\gamma} \in [1,\infty] \text{ since } \gamma \in [0,1] \tag{19}$$

$$\rho = \sqrt{\kappa^2 - 1} \tag{20}$$

with κ and ρ the center and radius of the circle respectively. The space inside (outside) the circle entails values of the magnitude of the active reflection coefficient lower (greater) than $\sqrt{\gamma}$.

Consequently, the arising inequality is

$$z_{\mathrm{in}}^{\mathrm{gp}}\overline{z_{\mathrm{in}}^{\mathrm{gp}}} - \kappa(z_{\mathrm{in}}^{\mathrm{gp}} + \overline{z_{\mathrm{in}}^{\mathrm{gp}}}) + 1 \leq 0 \tag{21}$$

where $z_{\mathrm{in}}^{\mathrm{gp}} = (Z_{\mathrm{in,lf}}^{\mathrm{gp}} + jX_r)/Z_l$.

Expanding (21) results in the following quadratic equation with respect to $w = \cot k_z^{\mathrm{dn}}h_g$:

$$(Z_l^2+X_r^2)C^2w^2+2X_rACw + A^2-2\kappa ABZ_l+(Z_l^2+X_r^2)B^2\le 0. \quad (22)$$

As we consider only isotropic materials ($\varepsilon_r \ge 1$) and scanning angles up to end-fire ($\theta < 90°$), it becomes apparent from (14)-(16) that $A>0$, $B>0$, & $C>0$. The roots of the 2nd order polynomial are

$$w_{1,2}=\frac{-X_rA\pm\sqrt{\Delta}}{C(Z_l^2+X_r^2)} \quad (23)$$

$$\Delta=(Z_l^2+X_r^2)[2\kappa AZ_l-(Z_l^2+X_r^2)B]B-Z_l^2A^2. \quad (24)$$

For the roots to be real numbers, $\Delta>0$ is required, leading to the condition

$$\kappa>\frac{Z_l^2A^2+(Z_l^2+X_r^2)B^2}{2ABZ_l(Z_l^2+X_r^2)}, \quad (25)$$

It can be proven for the right-hand side (RHS) of (25) that RHS >1, which is the case also for κ (19).

In (22), the quadratic coefficient $(Z_l^2+X_r^2)C^2$ is always positive, thus its solution can be written as

$$\frac{-X_rA+\sqrt{\Delta}}{C(Z_l^2+X_r^2)}\ge\cot k_z^{\text{dn}}h_g\ge\frac{-X_rA-\sqrt{\Delta}}{C(Z_l^2+X_r^2)}. \quad (26)$$

Only the left inequality is required to find the low-frequency bound. Since the low-frequency approximation is valid for $f<0.5f_0$, the longitudinal wavenumber in the substrate ranges up to $k_z^{\text{dn}}<\pi/2$. Therefore, $k_z^{\text{dn}}h_g\in[0,\pi/2]$ for $h_g<\lambda_g^{\text{dn}}/2$ which is well above the usual maximum value of $\lambda_g^{\text{dn}}/4$ used for the substrate's thickness. As a consequence, $\cot k_z^{\text{dn}}h_g$ is positive and continuous in our problem.

Therefore, to ensure the validity of (26), we need the larger root w_2 of (23) to be also positive, yielding

$$\kappa>\frac{A^2+(Z_l^2+X_r^2)B^2}{2ABZ_l}\ \text{or}\ X_r\le 0. \quad (27)$$

It should be noted that (27) is a more restrictive condition for κ than (25) when $X_l>0$. Both hold in general for realistic values of the involved parameters. Moreover, the lower root w_1 of (23) is negative when (27) holds, which means that the right inequality of (26) is satisfied.

The low-frequency limit is eventually derived as

$$f_{\text{lo}}=\frac{\cot^{-1}\frac{-X_rA+\sqrt{\Delta}}{C(Z_l^2+X_r^2)}}{2\pi h_g\sqrt{\varepsilon_r^{\text{dn}}-\sin^2\theta}}. \quad (28)$$

Matching a connected slot array under the assumption that it radiates in a homogeneous half-space is the best-case scenario since it removes the need for a multi-layer superstrate as an impedance transformer [14] and, thus, is not limited by the dispersion and the angle-dependence of the matching structure. Consequently, this simplifying conjecture ensures that (28) constitutes a bound on the performance of reflector-backed connected slot arrays.

TABLE I
CONFIGURATION OF THE UNIT-CELL OF FIG. 1

d	w_s	δ_s	h_g	$\varepsilon_r^{\text{dn}}$	$\varepsilon_r^{\text{up}}$	Z_l	X_r
$0.5\lambda_g^{\text{up}}$	$0.15\lambda_g^{\text{up}}$	$0.2\lambda_g^{\text{up}}$	$0.25\lambda_g^{\text{dn}}$	1	20	$70\,\Omega$	$-50\,\Omega$

λ_g^{up} (λ_g^{dn}) is the guided wavelength in the medium above (below) the radiation plane at the design frequency f_0.

IV. RESULTS

Further examination of (28) can provide additional insights and information on the operation principles of the connected slot array.

For example, the inverse relation between f_{lo} and h_g becomes immediately apparent. When there is no back reflector or $h_g\to\infty$, then there is no frequency limit or $f_{\text{lo}}\to 0$, as already known [15].

Similarly, the relative permittivity of the substrate $\varepsilon_r^{\text{dn}}$ determines the electrical length of h_g, hence, influencing f_{lo} accordingly.

A. Broadside Radiation

Assuming broadside radiation for simplification, we can study the relation of f_{lo} with other parameters such as $\varepsilon_r^{\text{up}}$ and X_r. It can be shown that, for both parameters, the low-frequency limit can be minimized. If we differentiate (28) with respect to $\varepsilon_r^{\text{up}}$ ($\partial f_{\text{lo}}/\partial\varepsilon_r^{\text{up}}$), the minimum point is found at

$$\varepsilon_r^{\text{up}}=\frac{\eta_0^2\kappa^2Z_l^2}{(Z_l^2+X_r^2)^2}, \quad (29)$$

where the low-frequency limit becomes minimum

$$\min_{\varepsilon_r^{\text{up}}} f_{\text{lo}}=\frac{\cot^{-1}\frac{(\rho Z_l-X_r)\eta_0}{(Z_l^2+X_r^2)\sqrt{\varepsilon_r^{\text{dn}}}}}{2\pi h_g\sqrt{\varepsilon_r^{\text{dn}}}}. \quad (30)$$

Then, by calculating $\partial f_{\text{lo}}/\partial X_r$, substituting $\varepsilon_r^{\text{up}}$ from (29), and finding its root, the minimum of f_{lo} with respect to both $\varepsilon_r^{\text{up}}$ and X_r is given by

$$\min_{\varepsilon_r^{\text{up}},X_r} f_{\text{lo}}=\frac{\cot^{-1}\frac{\eta_0}{2(\kappa-\rho)Z_l\sqrt{\varepsilon_r^{\text{dn}}}}}{2\pi h_g\sqrt{\varepsilon_r^{\text{dn}}}} \quad (31)$$

$$X_{r,\min}=(\rho-\kappa)Z_l \quad (32)$$

$$\varepsilon_{r,\min}^{\text{up}}=\left(\frac{\eta_0^2}{2Z_l(\rho-\kappa)}\right)^2. \quad (33)$$

Equations (32) and (33) indicate that the position of the minimum frequency limit depends on ρ and κ, which in turn are both functions of γ, as well as on Z_l. Therefore, we can see in Table II that $X_{r,\min}$ and $\varepsilon_{r,\min}^{\text{up}}$ are unaffected when either h_g or $\varepsilon_r^{\text{dn}}$ changes. Table II displays the minimum frequency limits and their location on the $X_r-\varepsilon_r^{\text{up}}$ space for the design of Table I (1st column) as well as of variations of it (2nd – 4th columns). We observe that $\varepsilon_{r,\min}^{\text{up}}$ takes high values that are difficult to realize with conventional dielectrics. Nevertheless, Fig. 4b showcases that the curve of f_{lo} for broadside flattens when $\varepsilon_r^{\text{up}}>10$. This means that the range of $\varepsilon_r^{\text{up}}$ can be restricted considerably without causing a substantial increase of

TABLE II
FREQUENCY LIMITS FOR THE UNIT-CELL FROM TABLE I FOR $|\Gamma_{\text{ACT}}| = -6\,\text{dB}$ ACCORDING TO (31) - (33).

	Table I	$Z_l = 120\,\Omega$	$h_g = 0.1\lambda_g^{\text{dn}}$	$\varepsilon_r^{\text{dn}} = 3$ *
$\min_{\varepsilon_r^{\text{up}}, X_r} f_{\text{lo}}/f_0$	0.078	0.133	0.196	0.134
$X_{r,\min}$	$-23.3\,\Omega$	$-39.9\,\Omega$	$-23.3\,\Omega$	$-23.3\,\Omega$
$\varepsilon_{r,\min}^{\text{up}}$	65.6	22.3	65.6	65.6

λ_g^{dn} is the guided wavelength in the substrate at the design frequency f_0.
* $\varepsilon_r^{\text{dn}}$ affects also the absolute value of h_g

f_{lo}. Furthermore, practically arbitrary $\varepsilon_r^{\text{up}}$ values can be obtained with properly designed ADLs [14].

Increasing Z_l results in a higher minimum f_{lo}, since at low frequencies, the real part of the connected slot's input impedance ranges around 40–80 Ω as illustrated in Fig. 3(a). A reduced h_g has the same effect on f_{lo}. This is expected since the ground plane is the principal cause limiting the bandwidth on the low end. Finally, an electrically denser substrate also results in increasing the minimum low frequency. The underlying reason is that a higher $\varepsilon_r^{\text{dn}}$ results in a larger portion of the slot's electromagnetic energy being directed to the substrate instead of being radiated. As a consequence, the cavity effect in the substrate is reinforced, decreasing the active input impedance of the connected slot array at low frequencies. Please note that a higher value for the $\varepsilon_r^{\text{dn}}$ translates to a thinner substrate since h_g is a function of the guided wavelength in the substrate λ_g^{dn}.

The insights obtained here studying the configuration of Table I radiating at broadside, extend to any configuration as well as to any steering angle.

B. Main Beam Steering

Equations (13) and (28) can be used to explore the behavior of the connected slot array when scanning. Calculating either the active input impedance or the low-frequency limit (Fig. 4), it becomes clear that the structure behavior changes substantially with the scanning plane. When steering over the H-plane ($\phi = 0°$), the unit-cell's $Z_{\text{in}}^{\text{gp}}$ remains essentially unaltered. This can be attributed to the fact that only the TE_{00} Floquet mode is excited when scanning over this plane, i.e., the electric field remains in parallel with the ground plane regardless of the scanning angle. Hence, in the low-frequency part of the spectrum, the physical problem does not practically change from the broadside case and both the active input impedance as well as the low-frequency limit for the two cases almost coincide.

On the other hand, when steering over the E-plane ($\phi = 90°$) the array couples with the TM_{00} Floquet mode, which has its E-field perpendicular to the steering direction and parallel to the scanning plane. Consequently, the wider the steering angle, the more perpendicular the electric field with respect to the backing reflector. As a result, wide scanning over the E-plane combined with low permittivity substrate excites surface waves in the form of TEM waves in the parallel plate waveguide (PPW) resembling substrate. This accounts for the significantly

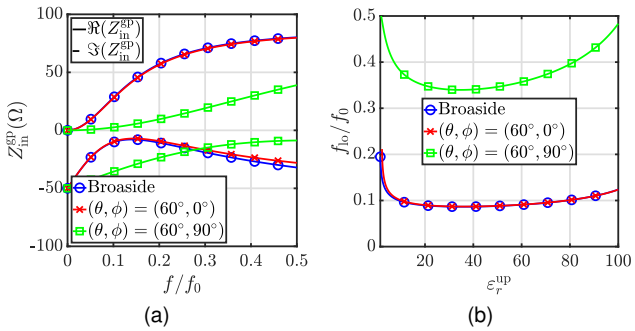

Fig. 4. Performance of the connected slot unit-cell with the design parameters as in Table I. (a) Active input impedance ($Z_{\text{in}}^{\text{gp}}$) and (b) low-frequency limit (f_{lo}) when steering the main beam over the principal planes. The curves of f_{lo} correspond to $|\Gamma_{\text{act}}| = -6\,\text{dB}$.

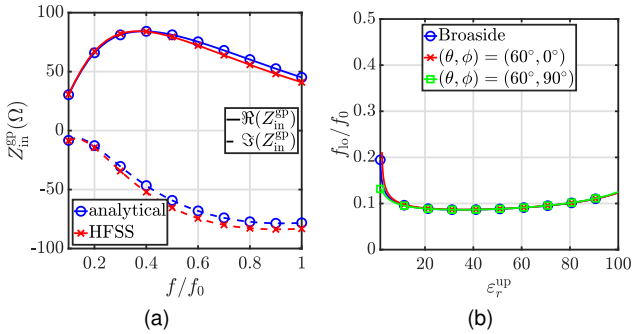

Fig. 5. Characterization of the connected slot unit-cell of Fig. 1b with the configuration of Table I: (a) active input impedance ($Z_{\text{in}}^{\text{gp}}$) for $(\theta,\phi) = (60°, 90°)$, (b) low-frequency limit (f_{lo}) when steering the main beam over the principal planes for $|\Gamma_{\text{act}}| = -6\,\text{dB}$.

reduced input impedance and higher frequency limits when scanning over the E-plane.

In practice, the surface waves are suppressed by placing via-walls in parallel to the slot as in [14]. Since this effectively blocks any wave propagating along the y-axis, it mathematically corresponds to imposing the wavenumber along this direction as zero $k_{y0} = 0$ when calculating $G_{xx,\text{dn}}^{HM}$. The modified unit-cell is illustrated graphically in Fig. 1b.

Using (12) with $k_{y0} = 0$ for $z < 0$, the active impedance of this architecture can be computed. Figure 5(a) compares the analytically obtained $Z_{\text{in}}^{\text{gp}}$ with full-wave simulation by HFSS for steering along the E-plane. The close agreement between the two results validates our modeling of the perfect electric conductor (PEC) walls. Furthermore, comparing Fig. 4(a) to Fig. 5(a) shows that the presence of the metallic walls in the substrate impacts significantly the active input impedance for $(\theta,\phi) = (60°, 90°)$. This consideration does not affect the behavior of the antenna when scanning at broadside or over the H-plane, in which cases $\phi = 0°$ and $k_{y0} = 0$ either way.

For the unit-cell of Fig. 1b, the parameter C, equation (16), in the low-frequency analysis becomes

$$C' = \sqrt{\varepsilon_r^{\text{dn}} - \sin^2\theta\cos^2\phi} \tag{34}$$

and the low-frequency bound transforms into

$$f'_{\text{lo}} = \frac{\cot^{-1}\frac{-X_r A+\sqrt{\Delta}}{C'(Z_l^2+X_r^2)}}{2\pi h_g C'}. \tag{35}$$

Figure 5(b) provides the low-frequency bound versus $\varepsilon_r^{\text{up}}$, showing that it remains almost identical regardless of the scanning plane. The introduction of metallic walls avoids the excitation of guided modes and significantly improves the array performance in the low-frequency band when steering along the E-plane.

In [18], a wideband connected slot unit-cell with a sophisticated overlaying ADL stack-up is introduced. It demonstrates a 5:1 bandwidth for scanning up to 60° over both principal planes. Using (28), we can prove that this unit cell with these steering specifications is limited to a bandwidth of 2:1 when no metallic walls are placed in the substrate. Nonetheless, by considering PEC walls in the substrate, a maximum bandwidth of 8:1 is analytically calculated with (35). This is in agreement with the findings of [18], whereas, with a slight increase of the substrate thickness, even a 10:1 bandwidth is attainable as also suggested in [20]. This indicates that more wideband and wide-scanning connected slot arrays can be designed with further improvements on the structure.

According to the findings of our analysis, there are two main challenges; approximating the appropriate $\varepsilon_r^{\text{up}}$ and obtaining the necessary X_r. The first requires a very wideband impedance transformer, capable of operating efficiently at low frequencies, in order to match the active impedance of the unit-cell with the wave impedance in free space. Even more critical is the latter which is intertwined with the development of a feeding network able to function at low frequencies with minimal mismatch losses. To achieve that, the feed has to provide the right value of X_r, as calculated with (32), which will cancel the inductive effect of the ground plane allowing the array's operation near f_{lo}. Finally, the designer should bear in mind that the absolute bounds presented here do not account either for the real impedance transformer or the real feed. As a result, they provide essential insight and practical guidelines on how to improve the low-frequency operation of connected slot arrays but it would be extremely demanding to design and fabricate an array radiating at f_{lo}.

V. Conclusion

The present work provides an analytical formulation for a low-frequency bound of connected slot arrays. The final expression allows us to evaluate the effect of every geometrical parameter of the unit-cell on its bandwidth. The analysis showed that there are two main ways to increase the bandwidth. The designer can either increase the substrate's electrical thickness or find the optimal combination of the superstrate medium and the reactance of the feeding line. Moreover, employing the proposed formulation, we could study the impact of guided modes in the substrate between the ground plane and the radiation plane. We proposed suppressing these unwanted waves by adding metallic walls in the substrate. A rigorous description of the modified unit-cell is provided. The derived bounds suggest that such a unit-cell of a connected slot array can provide bandwidth of 10:1 with a field of view up to 60° in elevation in all azimuthal planes. The proposed analysis can be extended, by duality, to an array of connected dipoles.

Acknowledgments

The authors would like to thank Dr. Daniele Cavallo for the fruitful discussions and his insightful suggestions.

References

[1] H. Wheeler, "Simple relations derived from a phased-array antenna made of an infinite current sheet," *IEEE Trans. Antennas Propag.*, vol. 13, no. 4, pp. 506–514, Jul. 1965.

[2] R. He, H. Zhang, C. H. See, Y. Su, Y. Ma, D. Kong, X. Zhu, and R. Abd-Alhameed, "A 1x8 linear ultra-wideband phased array with connected dipoles and hyperbolic microstrip baluns," *IEEE Access*, vol. 6, pp. 52 953–52 968, 2018.

[3] A. D. Johnson, J. Zhong, S. Sekelsky, E. A. Alwan, and J. L. Volakis, "Dual-polarised wideband tightly coupled dipole array for airborne applications," *IET Microw. Antennas Propag.*, vol. 14, no. 12, pp. 1476–1480, Oct. 2020.

[4] M. Del Mastro, F. Foglia Manzillo, D. González-Ovejero, M. Śmierzchalski, P. Pouliguen, P. Potier, R. Sauleau, and M. Ettorre, "Analysis of circularly polarized CTS arrays," *IEEE Trans. Antennas Propag.*, vol. 68, no. 6, pp. 4571–4582, Jun. 2020.

[5] S. Zhou, M. Ettorre, and A. Grbic, "An 8 × 4 continuous transverse stub array fed by coaxial ports," *IEEE Antennas Wireless Propag. Lett.*, vol. 18, no. 6, pp. 1303–1307, Jun. 2019.

[6] R. W. Kindt and B. T. Binder, "Dual-polarized planar-printed ultrawideband antenna array on a triangular grid," *IEEE Trans. Antennas Propag.*, vol. 68, no. 8, pp. 6136–6144, Aug. 2020.

[7] D. Cavallo, W. H. Syed, and A. Neto, "Connected-slot array with artificial dielectrics: A 6 to 15 GHz dual-pol wide-scan prototype," *IEEE Trans. Antennas Propag.*, vol. 66, no. 6, pp. 3201–3206, Jun. 2018.

[8] M. Gustafsson, "Broadband Self-Complementary Antenna Arrays," in *Ultra-Wideband Short-Pulse Electromagnetics 8*, 1st ed., C. E. Baum, A. P. Stone, and J. S. Tyo, Eds. New York, NY, USA: Springer, 2007, pp. 17–24.

[9] B. Tomasic and H. Steyskal, "Minimum Q of the element in an infinite phased array - TMz case," in *Proc. 19th Int. Conf. Appl. Electromagn. Commun. (ICECom)*, Sep. 2007, pp. 1–8.

[10] ——, "Minimum Q of the element in an infinite phased array," in *Proc. IEEE Antennas Propag. Soc. Int. Symp.*, Jun. 2007, pp. 145–148.

[11] D.-H. Kwon and H.-C. Chang, "Bandwidth limitations of linearly polarized infinite planar phased arrays in free space," *IEEE Trans. Antennas Propag.*, vol. 63, no. 8, pp. 3423–3431, Aug. 2015.

[12] J. P. Doane, K. Sertel, and J. L. Volakis, "Matching bandwidth limits for arrays backed by a conducting ground plane," *IEEE Trans. Antennas Propag.*, vol. 61, no. 5, pp. 2511–2518, May 2013.

[13] ——, "Bandwidth limits for lossless, reciprocal PEC-backed arrays of arbitrary polarization," *IEEE Trans. Antennas Propag.*, vol. 62, no. 5, pp. 2531–2542, May 2014.

[14] W. H. Syed, D. Cavallo, H. T. Shivamurthy, and A. Neto, "Wideband, wide-scan planar array of connected slots loaded with artificial dielectric superstrates," *IEEE Trans. Antennas Propag.*, vol. 64, no. 2, pp. 543–553, Feb. 2016.

[15] A. Neto and J. J. Lee, ""Infinite bandwidth" long slot array antenna," *IEEE Antennas Wireless Propag. Lett.*, vol. 4, pp. 75–78, 2005.

[16] C. A. Balanis, *Antenna Theory: Analysis and Design*, 4th ed. Hoboken, NJ, USA: Wiley, 2016.

[17] D. Cavallo, A. Neto, and G. Gerini, "Green's function based equivalent circuits for connected arrays in transmission and in reception," *IEEE Trans. Antennas Propag.*, vol. 59, no. 5, pp. 1535–1545, May 2011.

[18] A. J. van Katwijk and D. Cavallo, "Analysis and design of connected slot arrays with artificial dielectrics," in *Proc. 2019 IEEE Int. Symp. Phased Array Syst. Technol. (PAST)*, Waltham, MA, USA, Oct. 2019, pp. 1–5.

[19] D. M. Pozar, *Microwave Engineering*, 4th ed. New York, NY, USA: Wiley, 2012.

[20] D. Cavallo, "Recent advances on wideband wide scanning connected slot arrays," in *Proc. 2022 IEEE Int. Symp. Phased Array Syst. Technol. (PAST)*, Waltham, MA, USA, Oct. 2022, pp. 1–3.